MENTATION PAGE

Form Approved
OMB No. 0704-0188

1. AGENCY USE ONLY (Leave blank)	2. REPORT DATE	3. REPORT TYPE AND DATES COVERED
	January 22, 1993	

4. TITLE AND SUBTITLE

Far Field Rotor Noise

5. FUNDING NUMBERS

DAAL03-90-G-0221

6. AUTHOR(S)

Valana L. Wells

7. PERFORMING ORGANIZATION NAME(S) AND ADDRESS(ES)

Department of Mechanical & Aerospace Engineering
Arizona State University
Tempe AZ 85287-6106

8. PERFORMING ORGANIZATION REPORT NUMBER

9. SPONSORING / MONITORING AGENCY NAME(S) AND ADDRESS(ES)

U. S. Army Research Office
P. O. Box 12211
Research Triangle Park, NC 27709-2211

10. SPONSORING / MONITORING AGENCY REPORT NUMBER

ARO 28002.1-EG

11. SUPPLEMENTARY NOTES

The view, opinions and/or findings contained in this report are those of the author(s) and should not be construed as an official Department of the Army position, policy, or decision, unless so designated by other documentation.

12a. DISTRIBUTION / AVAILABILITY STATEMENT

Approved for public release; distribution unlimited.

12b. DISTRIBUTION CODE

13. ABSTRACT *(Maximum 200 words)*

The work covered two main areas of research--the aerodynamics of rotor blades including viscous and high angle of attack effects and, secondly, the propagation of noise from the rotor blade, particularly the nonlinear propagation. The aerodynamics work included the development and testing of a Navier-Stokes computational solver for rotor blades which incorporates rotating, translating, flapping and feathering motions. Results, which focus on the British Experimental Rotor Programme (BERP) blade, clearly show the importance of including all motions in the calculation of aerodynamic forces. The acoustics research concentrates on the development of a method for computing the non linear propagation of acoustic signals in the atmosphere. The method is based on a boundary-element discretization of the time-dependent, nonlinear wave equation. Results, computed for a spherically symmetric domain, show an equivalence with Whitham's method up to the formation of a shock.

14. SUBJECT TERMS	15. NUMBER OF PAGES	16. PRICE CODE
	25	

17. SECURITY CLASSIFICATION OF REPORT	18. SECURITY CLASSIFICATION OF THIS PAGE	19. SECURITY CLASSIFICATION OF ABSTRACT	20. LIMITATION OF ABSTRACT
UNCLASSIFIED	UNCLASSIFIED	UNCLASSIFIED	UL

Far Field Rotor Noise

Final Report

Valana L. Wells

January 22, 1993

U. S. Army Research Office

Grant Number DAAL03-90-G-0221

Department of Mechanical and Aerospace Engineering
Arizona State University
Tempe, AZ

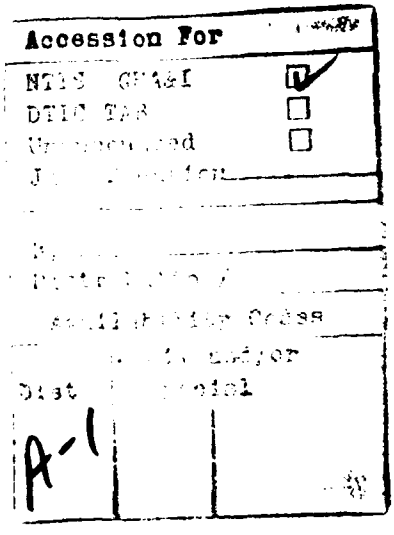

Abstract

The report outlines the methodology utilized and results acheived under the U. S. Army Research Office grant number DAAL03-90-G-0221. The work covered two main areas of research—the aerodynamics of rotor blades including viscous and high angle of attack effects and, secondly, the propagation of noise from the rotor blade, particularly the nonlinear propagation. The aerodynamics work included the development and testing of a Navier-Stokes computational solver for rotor blades which incorporates rotating, translating, flapping and feathering motions. Results, which focus on the British Experimental Rotor Programme (BERP) blade, clearly show the importance of including all motions in the calculation of aerodynamic forces. The acoustics research concentrates on the development of a method for computing the nonlinear propagation of acoustic signals in the atmosphere. The method is based on a boundary-element discretization of the time-dependent, nonlinear wave equation. Results, computed for a spherically symmetric domain, show an equivalence with Whitham's method up to the formation of a shock.

Contents

List of Figures

1 Description of Research

1.1 Aerodynamics of Advanced Rotor Blades

This section summarizes the developed Navier Stokes solution method which, apparently, closely resembles that employed by Duqué[1]. The text also describes the grid and its generation. The current grid provides a notable improvement over the more typical C–H grids utilized in previous studies of the BERP blade, since it can more completely describe the highly-swept BERP blade at the tip, a critical part of the geometry.

Though the method does provide improvements, it should be noted that some incompleteness remains. The first problem area involves the wake effect. It has become commonplace to account for the effect of the rotor wake by introducing a downwash velocity at the blade surface as, essentially, a boundary condition. This surface velocity, computed independently using a code such as CAMRAD, can be uniform, vary radially, or vary in both radial and chordwise directions, depending on the degree of complexity sought. However, the programs which generate the induced velocities cannot at present handle odd geometries or high blade angles, and are of little use for predicting the induced velocities at the BERP surface. The current method ignores the effect of the wake, except the small part of it contained within the computational grid. It is, of course, impossible to predict the pressures, forces, and moments which would arise on an actual lifting blade under the prescribed flow conditions when the wake is not considered. However, there appears to be no computationally realistic way to include any reasonably accurate wake effect at this time. Ignoring the wake should not significantly change the basic characteristics of the flow field, as observed by Tsung *et. al.*[2] who use only a constant correction factor for the velocity at the blade surface. Consideration of this wake effect was not at issue for Duqué who studied only rectilinear flight regimes.

The remaining area of concern involves the turbulence modeling. It appears, through a study of the literature and through discussions with experts in the field, that there remains a fair amount of disagreement regarding the accuracy and applicability of the various turbulence models. It seems that no model currently exists which will reliably predict flow

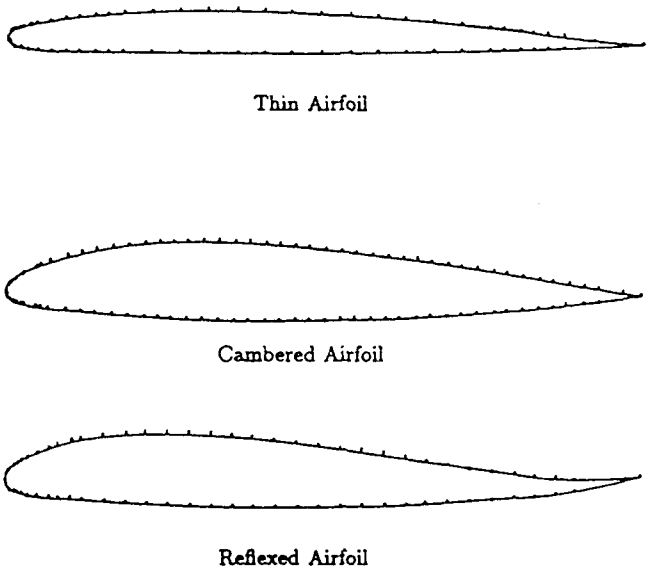

Figure 1: Rotor airfoils used in the current study.

separation or shock-wave location under a wide range of conditions. It also appears in doubt as to which model performs best under the conditions under study here. Based on some previous results of Lomax and Mehta[3] and Degani and Schiff[4], and because of its relative simplicity, the Baldwin-Lomax turbulence model was chosen for use in this study. The primary drawback of this model seems to be in predicting shock location on transonic airfoils. The previously mentioned references indicate that, at least in some cases, the model works well in predicting separation on airfoils and bodies at high incidence.

The advanced-geometry rotor blade under current study represents only an approximate rendition of the true BERP blade. Though the blade planform is available in the public domain, the blade airfoils and the twist of the rotor inboard of the tip paddle were unavailable. The rotor studied here had the exact BERP planform, but airfoils were defined based only on the sketches published by Perry[5]. Though the actual BERP blade has inboard twist, the current blade has none. Thus, the results published here cannot duplicate the performance of the actual BERP blade. However, since one objective is to determine planform effects on

the flow field surrounding the rotor blade, the actual airfoils used should have only secondary effect on the desired results. Figure 1 shows the geometry of the airfoils used in generating the results presented here. One set of calculations was performed on a rotor with a BERP tip but with NACA 00xx airfoils, where xx refers to the thickness ratio at a particular location. The thickness distributions for both sets of airfoils was the same.

The simplest way to create a grid for solving rotor-blade aerodynamics problems consists of generating two-dimensional C-grids at various radial locations and then stacking them in the spanwise direction. For most conventional rotor geometries, this approach presents no difficulty. Because of its highly-tapered tip, however, using this approach for the BERP blade leads to extremely small cell sizes near the blade tip where the chord becomes very small. In fact, the length of the chord on the actual blade planform goes to zero at the tip—a geometry which cannot be handled by the C–H generation method described above. An approach to avoiding the difficulties at the tip involves "clipping" the blade at some inboard, finite-chord station. This approximation causes two problems. Firstly, it causes the loss of the effects of the tip regions of the blade which may be of great importance. Secondly, even though the blade is clipped at some non-zero chord position, for the geometry to be even closely approximated, the chord-length must necessarily be quite small. This causes a very dense clustering of grid points near the tip, extending radially to the far field. In effect, such a grid wastes grid points in areas where they are not needed and puts a severe restriction on the maximum allowable time step because of the small cell size.

The problems due to clipping can be remedied by constructing a grid in which the "spanwise" stations on the blade surface can be rotated in any direction, specified by giving leading and trailing edge positions of a station rather than a single spanwise location. The last station on the blade can thus be made parallel to the actual blade tip. Near the tip, both on and off the blade, the sections are specified to "fan" into the inner and outer parallel sections. The upper and lower surfaces at any station on the blade are interpolated from the actual airfoils using bilinear surface patches. Figure 2 shows a computational grid on the blade surface.

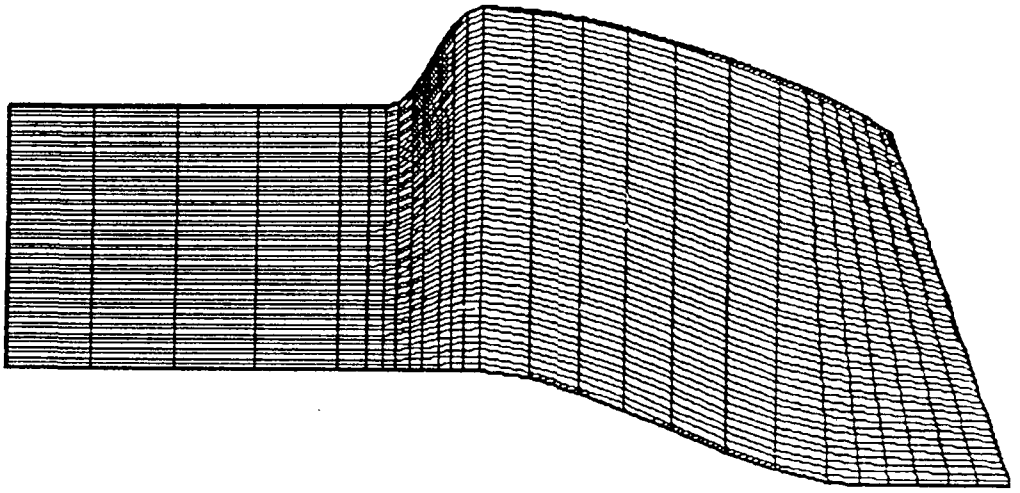

Figure 2: Surface grid on the BERP blade tip.

The only equations suitable for highly separated flows and amenable to present computers are the Reynolds-Averaged Navier-Stokes equations. An implicit, time accurate LU decomposition method proposed by Obayashi and Fujii[6] is adapted to solve for the flow properties near and on the rotor blade. Benefits from this procedure include less computational work as well as less required storage than conventional ADI methods. Furthermore, it does not require special differencing because of the three-dimensionality of the flow, and the code to implement it is easily vectorized. A local geometrical time step is used for steady-state problems to increase the convergence rate. Choosing a constant time step will produce a time-accurate solution for unsteady problems.

The solution method handles the blade motion by imparting a velocity relative to a fixed, inertial reference frame to each point on the grid. Grid velocities appear in the governing equation, derived in a fixed frame of reference, as control volume velocities. For hover and simple forward flight cases, the expression for these is commonly known and fairly straightforward. If, however, the blade undergoes flapping and feathering motions, as well as rotation and forward flight, the transformation from a grid-fixed system to a space-fixed one becomes much more complex. Appendix A contains a derivation of the grid velocities relative to a fixed coordinate system for a pitching and flapping rotor blade. At this time,

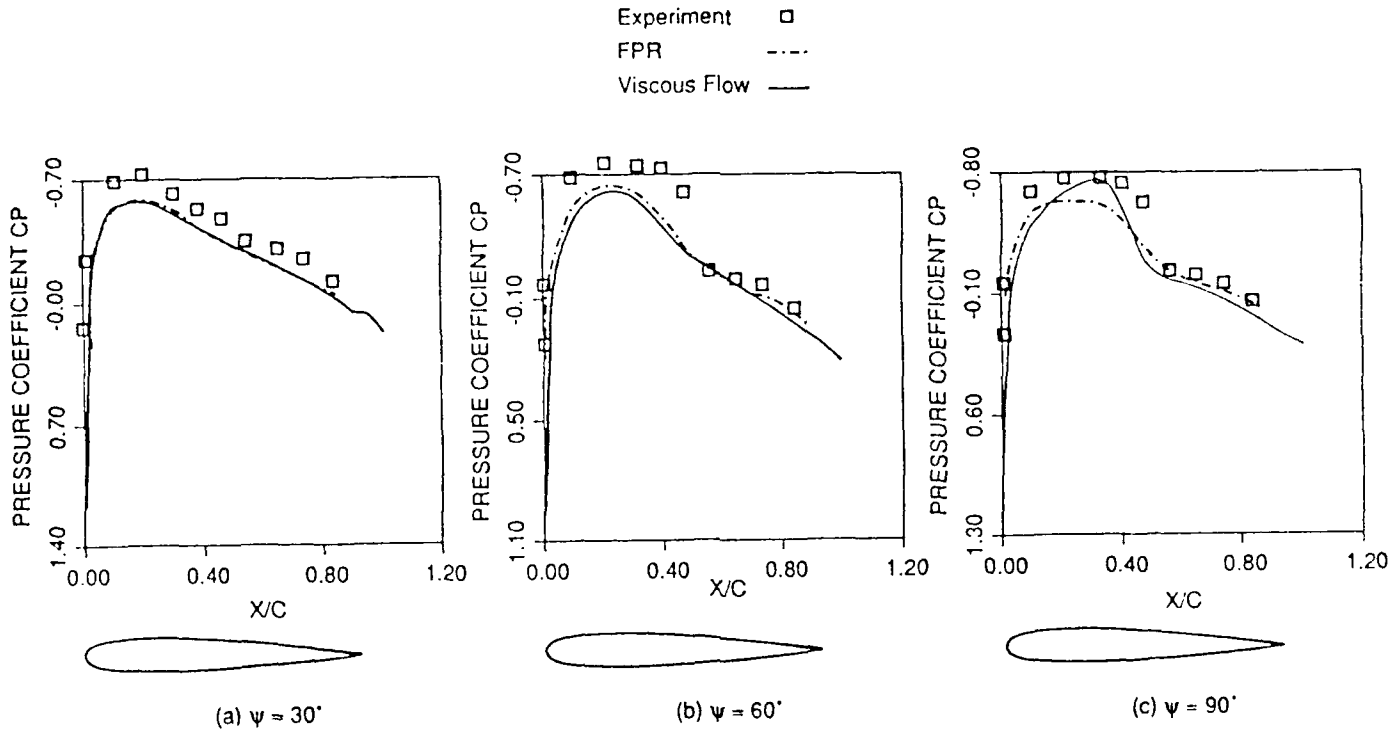

Figure 3: Comparison of current results with previous, inviscid calculation and with experiment—rectangular blade, $M_{tip} = .7$, $\mu = .3$.

the motion is constrained to that for a rigid rotor pitching about any radial axis, but flapping about a hinge with no offset. Including a hinge offset is not difficult; including flexibility in the blade requires much information about the structural modes of the rotor and introduces a complexity well beyond the scope of the current study.

1.1.1 Results

Several code verification cases were run; those shown in figure 3 compare the results of the current code with those computed by FPR[7], a transonic, full-potential rotor analysis code. Some experimental data is also included. The figure shows pressure coefficients for an untwisted rectangular rotor blade with a constant NACA 0012 airfoil at zero angle of attack, with rotational tip Mach number of .7 and advance ratio .3. Three azimuthal angles are included, and the radial position is at 89% of the maximum. The data shows good correlation with the results of FPR and fairly good correlation with the experiment.

In order to compare with the results of Duqué, the code was run for the BERP planform

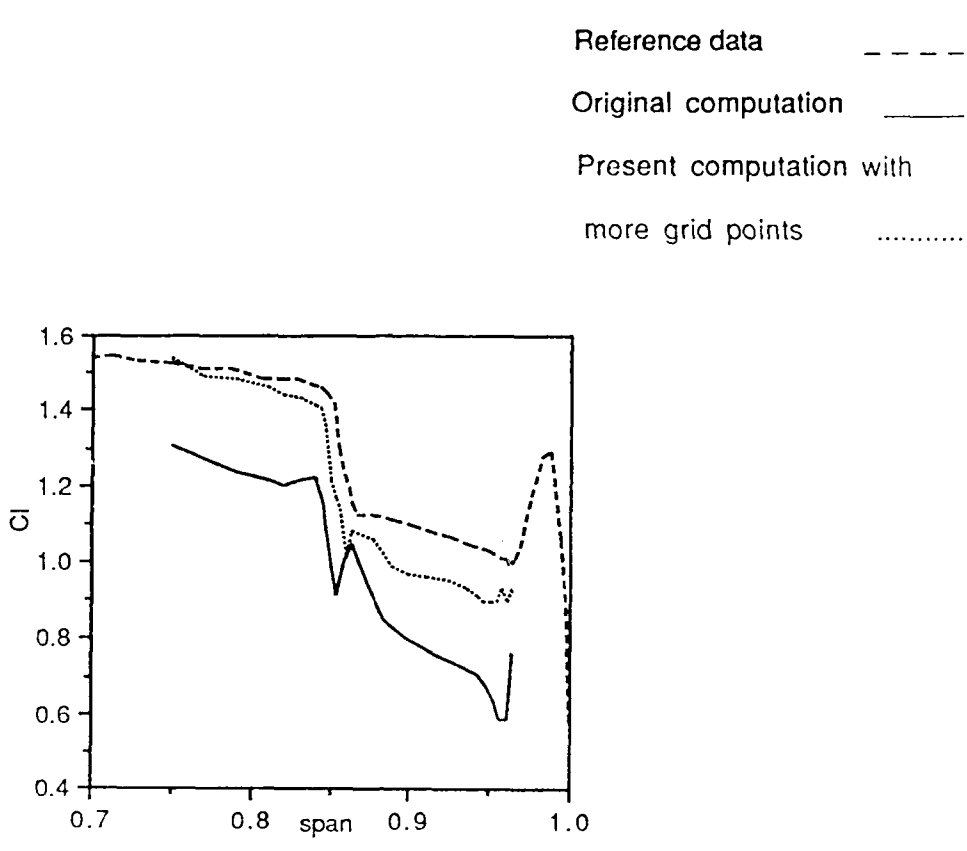

Figure 4: Lift Coefficient in Uniform Flow, $M = .2$, $\alpha = 13°$.

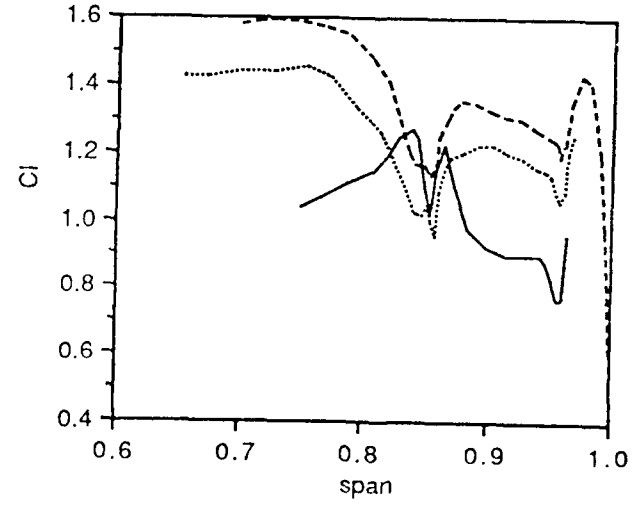

Figure 5: Lift Coefficient in Uniform Flow, $M = .2$, $\alpha = 20°$.

in uniform flow (non-rotating) at .2 Mach number and 13° and 20° angle of attack. Figures 4 and 5 show the computed lift coefficients for these cases. The current results are shown for two grid sizes. The original grid was the largest possible for the memory available on the Arizona State University Cray X-MP. When the NASA Ames Cray Y-MP became available, a grid convergence study was undertaken. It was determined that an increase of 21% in the number of grid points was required for convergence with the blade at 13° angle, and an increase of 81% was required with the blade at 20°. The maximum grid size utilized was $123 \times 45 \times 43$ points in the wrap-around, perpendicular, and spanwise directions, respectively.

Several discrepancies exist between the results of Duqué and the current ones. These occur, first and formost, because of the differing airfoils. Additionally, since Perry's[5] and Duqué's descriptions of the airfoil thickness and its distribution along the blade differ, some variations in the lift distributions could occur simply because of the differing thicknesses. This would be particularly apparent at high angles of attack. Nevertheless, the major trend of lift coefficient with span is consistent between the two results. The 13° case was run with NACA 00xx symmetric airfoils, as well as with the BERP-like airfoils. Results from these calculations show virtually the same dependence on span, but at a slightly lower value of c_ℓ.

A major thrust of the work described herein is to determine the effect on the advanced rotor blade of the unsteadiness, not only due to forward flight, but also incurred because of the blade motions. Therefore, the Navier-Stokes code was written in such a way as to easily incorporate arbitrary blade motion through time dependent grid velocities. Appendix A describes the derivation for the grid velocities including blade feathering and flapping as well as the rotational and translational motions. The figures below show results for a BERP-like blade in forward flight with $\mu = .25$ and hover tip Mach number equal to .65. The prescribed collective and cyclic pitch was given as $\theta = 10 - 10 \sin \psi$, where θ is given in degrees. For given blade properties, it is quite possible to solve for the blade position —*i.e.*, the blade flapping —as a consequence of the computed forces if it is assumed that most of the lift on the blade comes from the outer portions over which the computation is carried out. This does, however, require the numerical solution of yet another differential equation which

describes the time-dependent blade motion. In order to avoid the additional complexity (and additional computation time) of including the blade dynamics at this initial stage of development, the flapping angle was prescribed to be $\beta = 5 - 5\cos\psi$. This flapping schedule is not necessarily realistic, especially for the large cyclic pitch introduced above. Nevertheless, it does provide a vehicle for examining the flow response to the type of unsteady motions experienced by a rotor blade. The flapping and feathering are given with respect to the shaft axis.

Though it is not necessarily valid to compare the results from the rotor in forward flight with no motion to those from the rotor with flapping and feathering, the comparison will, nonetheless be made. As shown in the figures, the prescribed motions cause large changes in the pressure distributions on the rotor blade at all radial stations. The illustrated pressure distributions are shown for radial positions at the notch and in the middle of the paddle.

1.1.2 Conclusions

The developed code provides a robust method for determining the forces on a rotor blade undergoing general motion. The current code could be enhanced by developing a manner in which to include the effects induced by the wake, a task which cannot be completed utilizing current methodology. Though uncertainty is introduced through use of a turbulence model, little can be done to ameliorate this in the absence of a more exact closure procedure.

The presented results concur with some previously published ones and introduce some additional conclusions with regard to the aerodynamic characteristics of the BERP rotor blade:

1. At high angles of attack, the blade produces a large, stable attached vortex at the tip.

2. The notch does seem to play a role in BERP aerodynamics—a vortex is produced at the notch which trails into the wake. This vortex does not appear to remain attached to the blade, although, at a 20° angle of attack, there may be some small region of attachment. The notch seems to provide a stall barrier for the inboard trailing-edge stall at $\alpha = 13°$ and for the large-scale separation at $\alpha = 20°$.

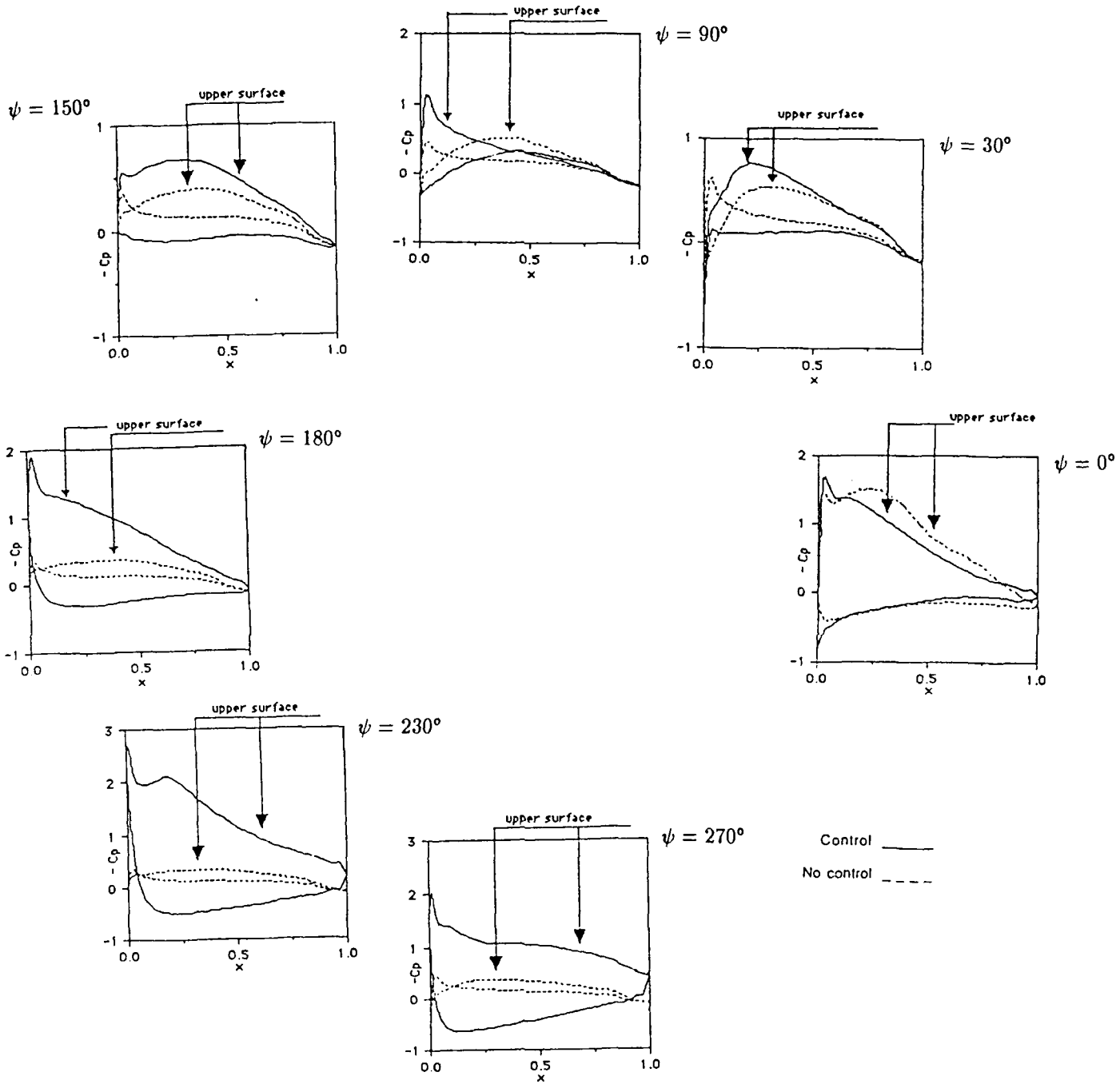

Figure 6: Pressure Distribution on BERP blade—Forward Flight, with and without motion, 85.5% radius.

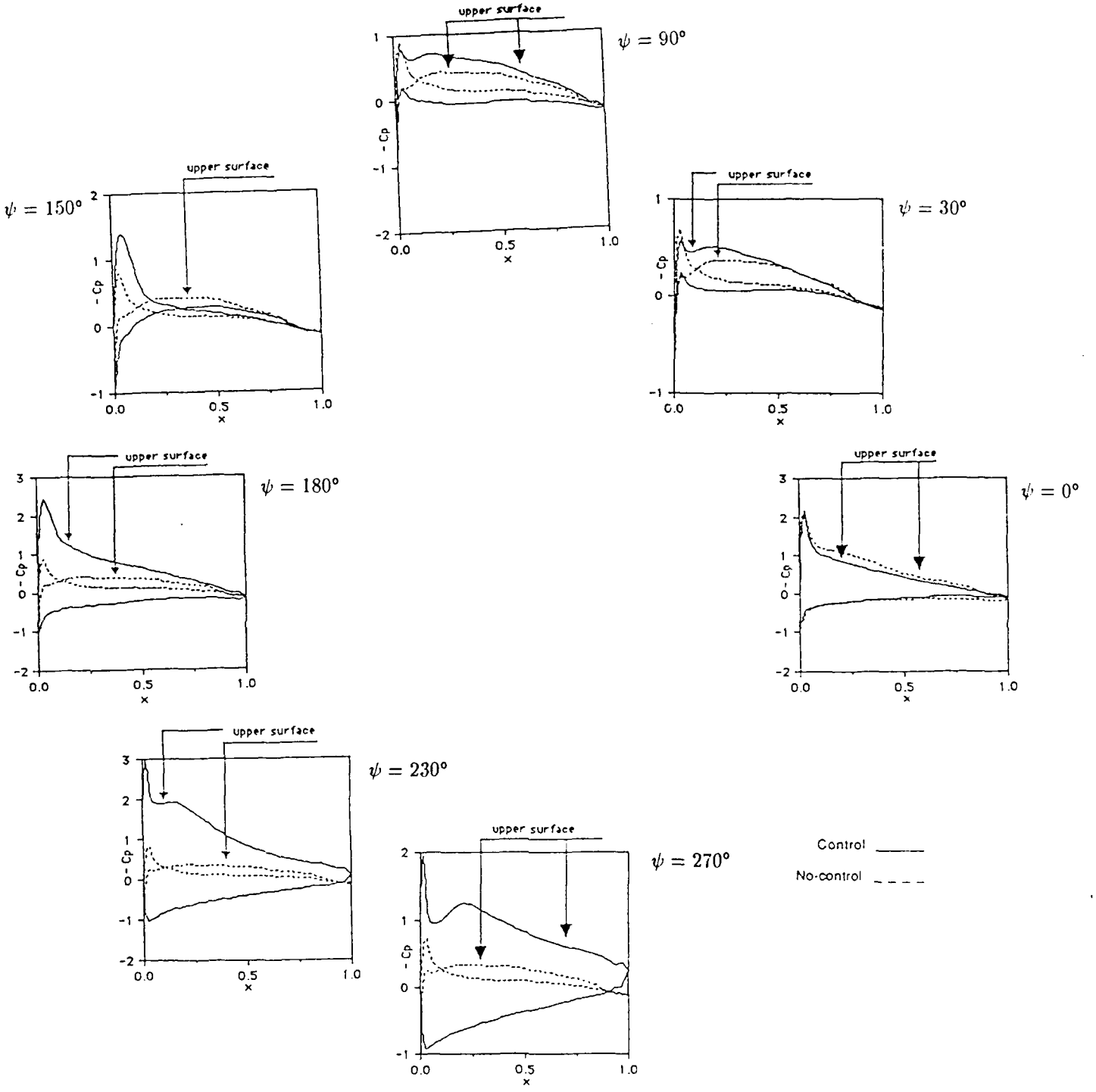

Figure 7: Pressure Distribution on BERP blade—Forward Flight, with and without motion, 90% radius.

3. The major features of the aerodynamics of the paddle section are unaffected by airfoil section.

4. Feathering and flapping motions greatly affect the loading on the blade.

1.2 Nonlinear Propagation of Acoustic Waves

Whitham[8] and others have shown that, in situations where the forces due to acoustic pressure disturbances overshadow those caused by dissipative processes, any acoustic signal will experience a deformation from the initial waveform. In the absence of dissipation, the signal will eventually steepen and form a shock due to the nonlinear nature of the real atmosphere in which the signal travels. Though the amplitude of a traveling acoustic wave decreases with distance from the source of the disturbance, the deformation of the wave becomes more pronounced as it travels farther and farther from the position of its inception. Consequently, as long as the disturbance is loud enough at the source (such as that produced by a fast-moving rotor blade), the signal will exhibit nonlinear steepening, especially as the wave travels to the far field.

Several methods are available for computing the wave field produced by an acoustic disturbance. The most widely attempted involves a finite difference approach, and Baeder[9] has enjoyed some success using this method. Finite differencing requires the use of large, dense grids, and it tends to subdue propagating disturbances because of the inherent artificial damping resulting from discretizing the partial derivatives of the governing equation. There are techniques available for reducing or eliminating this extraneous damping, but the current research centers on developing a methodology for solving the integral rather than the differential form of the nonlinear wave equation. Numerical solution of the integral equation involves summations rather than differences and is, therefore, less subject to discretization errors and should require fewer grid points for an accurate solution.

The complete acoustic analogy equation, including non-linear effects, can be generically written as

$$\rho(\mathbf{x},t) - \int_{-\infty}^{\infty} [f(\mathbf{x},\mathbf{y},\rho(\mathbf{y},\mathbf{t}))]_{t=\tau}\, dV(\mathbf{y}) = 0, \qquad (1)$$

where ρ represents the acoustic (disturbance) density. Strictly speaking, the function f in the integrand depends not only on ρ, but also on the variables p (acoustic pressure) and $\mathbf{v}$ (disturbance velocity). Additional auxiliary equations, the choice of which depends on the assumptions and simplifications of the problem, provide the relationships between p, $\mathbf{v}$, and ρ. For example, the isentropic relation provides p as a function of ρ when the isentropic assumption is invoked. The other governing equations give velocity—for one-dimensional propagation, the continuity equation proves sufficient for finding the velocity with density given.

Equation 1 appears similar to a Volterra integral equation of the second kind but differs in that the variables in the integrand must be evaluated at the *retarded* time, $\tau = t - |\mathbf{x} - \mathbf{y}|/c_0$, where, as is customary, $\mathbf{x}$ represents observer position, $\mathbf{y}$ represents source position (in the integrand), and c_0 is the ambient speed of sound. An approximation to eq. 1 for the density at N x-locations (grid size, N), can be written as

$$\rho_i(t) - \sum_{j=1}^{N} g(\rho_j(\tau)) \int_{-\infty}^{\infty} K(\mathbf{x}, \mathbf{y}) dV(\mathbf{y}) = 0, \tag{2}$$

where the integrand of eq. 1 is replaced with $g(\rho(\mathbf{y}, \tau))K(\mathbf{x}, \mathbf{y})$, and i runs from 1 to N. Equation 2 appears very similar to a boundary element approach to solution of integral equations except that the density within the summation must be computed at the retarded time. Equation 2, then, represents a set of N equations (one for each of the N grid points) with N^2 unknowns—the N ρ_i's and the $N(N-1)$ ρ_j's.

In order to make the computational procedure more tractable, a simpler form of eq. 1 was utilized to solve for the wave field produced by a pulsating sphere:

$$4\pi\varphi = \int_S \left[\frac{v_n}{R}\right] dS + \int_S \left[\frac{\partial \varphi}{\partial t}\right] \frac{1}{R} \frac{\partial R}{\partial n} dS + \int_S \left[\frac{\varphi}{R^2}\right] \frac{\partial R}{\partial n} dS + \frac{\gamma - 1}{2} \int_V \frac{\partial}{\partial t} \left[\left(\frac{\partial \varphi}{\partial t}\right)^2\right] \frac{1}{R} dV. \tag{3}$$

Equation 3 is equivalent to the transonic small-disturbance equation for aerodynamics, and all quantities have been made dimensionless. The square brackets indicate evaluation at the retarded time. In eq. 3, φ represents the velocity potential, v_n is the normal velocity of a

surface bounding the field, and R is the distance between an observer point and a point in the field. The equation can be discretized for an $N \times M$-point grid as

$$4\pi\varphi_i(t) = \sum_{j=1}^{N} \frac{\partial\varphi_j(\tau)}{\partial n} \int_{S_j} \frac{1}{R_{ij}} dS + \sum_{j=1}^{N} \frac{\partial\varphi_j(\tau)}{\partial t} \int_{S_j} \frac{\cos\alpha_{ij}}{R_{ij}} dS + \sum_{j=1}^{N} \varphi_j(\tau) \int_{S_j} \frac{\cos\alpha_{ij}}{R_{ij}^2} dS$$
$$+ (\gamma - 1) \sum_{j=1}^{N} \sum_{k=1}^{M} \frac{\partial^2\varphi_{jk}(\tau)}{\partial t^2} \frac{\partial\varphi_{jk}(\tau)}{\partial t} \int_{V_{jk}} \frac{1}{R_{ijk}} dV. \quad (4)$$

Equation 5 represents, effectively, $N \times M$ equations with $(N \times M)^2$ unknowns, just as described above with regard to eq. 2. In the above, α_{ij} is the angle between the normal to the bounding surface and the vector, $\mathbf{x} - \mathbf{y}$.

Groenenboom[10] suggests using a linear interpolation of the unknown variable (in this case, φ_i) as a function of t in order to estimate its values at the appropriate retarded times. However, the linear interpolation for φ gives a constant value for $\partial\varphi/\partial t$ for the duration of a given time step, Δt, and therefore, gives a zero value for the second derivative with respect to t except at times given by $n\Delta t$ (n an integer) when φ_{tt} is undefined. For the linear problem, in which φ_{tt} is not required, this simple interpolation may work quite well, but it is obviously not suited to the nonlinear case. It was decided, therefore, to use a fast Fourier transform to interpolate between known times to determine the values of φ at the correct retarded times. The known, linear solution is used as a starting solution for the iteration.

Figure 8 shows results of the initial computations for the pressure as a function of radial distance for a Mach number on the surface of the sphere of .2 for both 40 and 60 grid points in the radial direction. The figure indicates little difference between the results for the two grid sizes. Additionally, the figure compares the results to the solution calculated using the classical method of Whitham adapted to the current problem involving a continuous wave train in three dimensions. The computed results appear to exhibit the classical problem with using too few Fourier coefficients to resolve the waveform. An attempt to solve this problem by simply doubling the number of Fourier coefficients results in a divergence of the iteration scheme.

Using the Fourier transform to approximate the interim solution after each iteration has the advantage that the time derivatives in eq. 5 are as easily estimated as the potential

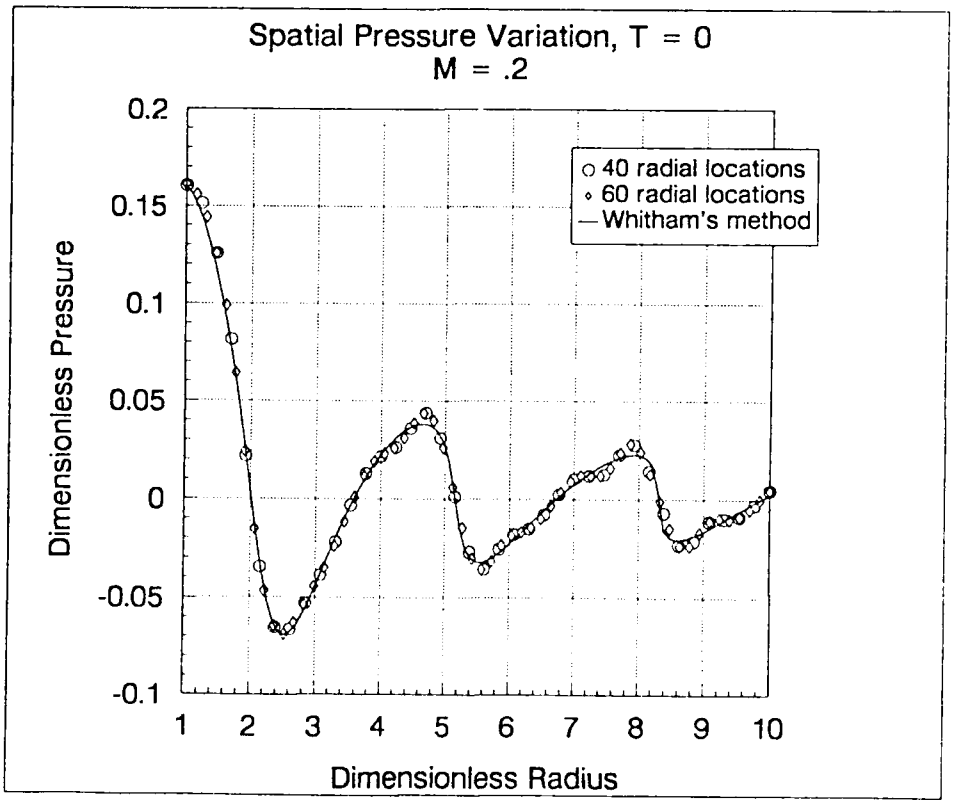

Figure 8: Solution at $t = 0$ for four Fourier terms.

function itself, and no numerical approximation to derivatives is required. However, each component of the Fourier series is multiplied by its frequency when the first derivative is taken and by the frequency squared for the second derivative. This procedure tends to exagerate any errors in the coefficients of the higher frequencies, especially in the nonlinear term which contains the product of the first and second derivatives of the velocity potential. Consequently, including additional, higher frequencies in the Fourier approximation to the velocity potential leads to the dominance of errors in these frequencies. As the nonlinear component of the potential becomes more pronounced, such as when the Mach number of the initial disturbance increases or the distance from the source surface becomes large, the importance of the high frequencies and, thus of their errors, also increases.

Figure 9 shows the computational results from the same case as before, but with eight terms in the Fourier series and using a technique to smooth the high frequencies. The smoothing method, due to Lanczos[11], averages the value of the signal over the smallest interval (Δt), or highest frequency, in the series. The technique appears to damp out high-

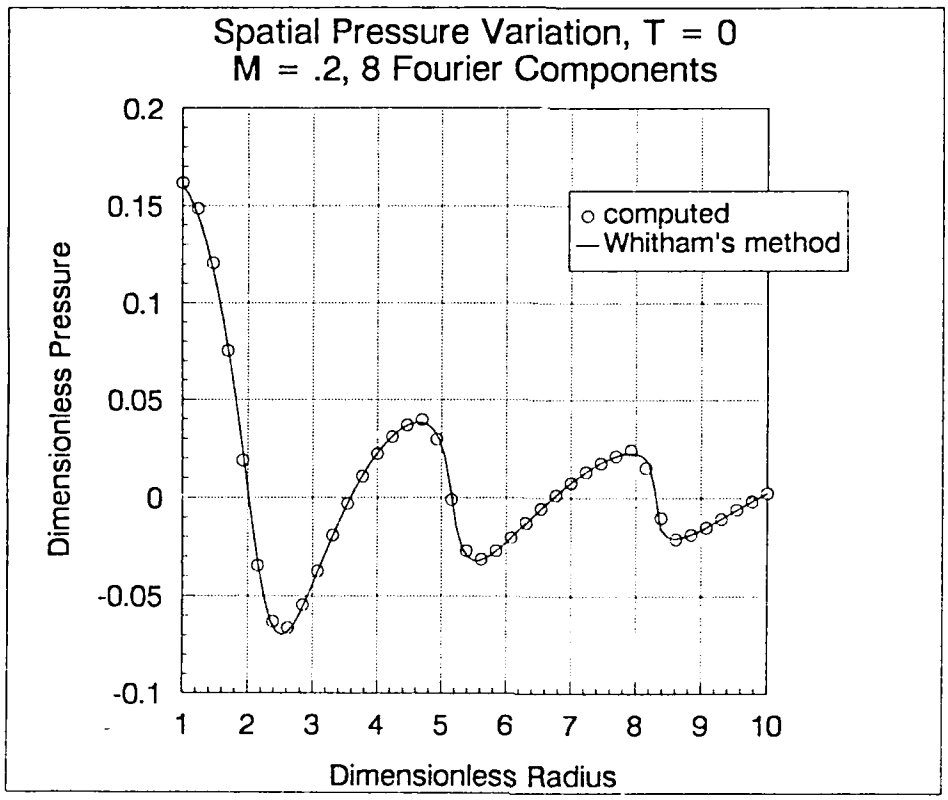

Figure 9: Solution at $t = 0$ for eight Fourier terms with Lanczos smoothing.

frequency errors up to the point where a shock (or a near-shock) appears in the waveform. As shown in the figure, the computed values compare well with the Whitham solution.

1.2.1 Conclusions

The developed computational method appears to provide a means for accurately predicting the nonlinear propagation of an acoustic signal. Because the nonlinear effect of steepening becomes progressively more apparent as the wave travels outward from the source, the effect will have increased importance in the far field. Though, as the figures show, the method gives good results for some cases, improvements must be made in order to handle more general conditions. Some of these include:

1. Once a shock (or at least a very large pressure gradient) appears in the outward-travelling wave, the Lanczos smoothing is not sufficient to supress the error in the high frequencies of the Fourier series approximation to the waveform. Therefore, some

other means for either smoothing the Fourier representation or even for approximating the function must be attempted. A suggested smoothing technique is the filtering of the waveform resulting from calculations at a given iteration before using it to compute values at the next iteration. It may be more appropriate to utilize a different interpolation method altogether for determining the values of the potential at the retarded times, although performing an FFT is very fast relative to polynomial spline fitting, for example.

2. The method has, at present, only been tested for the very simple case of the pulsating sphere, which is both stationary and spherically symmetrical. The code must be adapted to account for more general geometries which do not necessarily exhibit simplifying symmetries, and for moving sources which are of interest in the calculation of helicopter rotor noise. Though neither of these adaptations modifies the basic method, which is a solution to eq. 3, the new geometry and retarded planform calculations add considerable complexity to the actual computer code.

3. The iteration procedure, sometimes termed *functional iteration*, seems to be painfully slow in its convergence characteristics. The more standard methods for improving the convergence, such as Newton-Raphson or secant methods, are not practical for such a large system of equations. Nevertheless, to make the solution method feasible, particularly for more complicated problems with larger integration grids, its convergence rate should be enhanced.

2 Supported Personnel and Publications

The grant supported Dr. V. Wells, the principal investigator, at 14% time during the academic year and for two months during the summer. Dr. G. Abdy, who developed and tested the Navier-Stokes code, was supported part-time during the first year of the grant. Dr. Abdy received his Ph.D. degree in August of 1992. Mr. Fred Sellin, a Masters' degree candidate, was supported at 50% time from January, 1991 to October, 1992.

The research supported by the grant has thus far resulted in one publication:

> Abdy, G. and Wells, V., "A Numerical Study of Advanced Rotor Blades," in *Proceedings of the International Technical Specialists Meeting on Rotorcraft Acoustics and Rotor Fluid Dynamics*, American Helicopter Society and The Royal Aeronautical Society, October 1991.

It is anticipated that the research performed under this grant will form the basis for several forthcoming publications.

References

[1] Duqué, Earl P. N., A Numerical Analysis of the British Experimental Rotor Program Blade, In *Proceedings of the 45th Annual Forum*, American Helicopter Society, 1989.

[2] Tsung, Fu-Lin, Liou, Shiuh-Guang, Komerath, Naryanan M., and Sankar, Lakshmi N., Computation and Measurement of the Flowfield Near a Swept Rotor Blade Tip in Hover, In *Proceedings of the 46th Annual Forum*, American Helicopter Society, 1990.

[3] Lomax, Harvard and Mehta, Unmeel B., Some Physical and Numerical Aspects of Computing the Effects of Viscosity on Fluid Flow, In Habashi, W. G., editor, *Computational Methods in Viscous Flows*, pp. 1–50, Pineridge Press, Swansea, U.K., 1984.

[4] Degani, D. and Schiff, L. B., Computation of Supersonic Viscous Flows Around Pointed Bodies at Large Incidence, *AIAA-83-0034*, 1983.

[5] Perry, F. J., Aerodynamics of the Helicopter World Speed Record, In *Proceedings of the 43rd Annual Forum*, American Helicopter Society, 1987.

[6] Obayashi, S. and Fujii, K., Computation of Three Dimensional Viscous Transonic Flows with the LU Factored Scheme, *AIAA-85-1510*, 1985.

[7] Strawn, R. C. and Caradonna, F. X., Conservative Full-Potential Model for Unsteady Transonic Rotor Flows, *AIAA Journal*, Vol. 25, February 1987, pp. 193–198.

[8] Whitham, G. B., On the Propagation of Weak Shock Waves, *Journal of Fluid Mechanics*, Vol. 1, 1956, pp. 290–318.

[9] Baeder, J.D., Euler Solutions to Nonlinear Acoustics of Non-Lifting Rotor Blades, In *Proceedings of the International Technical Specialists Meeting on Rotorcraft Acoustics and Rotor Fluid Dynamics*, American Helicopter Society and Royal Aeronautical Society, October 1991.

[10] Groenenboom, Paul H. L., The Application of Boundary Elements to Steady and Unsteady Potential Fluid Flow Problems in Two and Three Dimensions, *Applied Mathematical Modelling*, Vol. 6, February 1982, pp. 35-40.

[11] Hamming, R. W., *Numerical Methods for Scientists and Engineers*, Chapter 32, Dover Publications, 1986.

A Derivation of Grid Velocities for a Rotor Undergoing Feathering and Flapping Motions

The derivation considers a rotor blade undergoing four basic types of motion. These include 1) forward flight at uniform velocity, 2) rotation about a hub axis with constant angular velocity, 3) feathering about an axis parallel to the blade span, and 4) flapping about a hinge at the hub. Because the code requires knowledge of the grid velocity with respect to a fixed, inertial coordinate system, the above motions must be described as such but in terms of coordiates on the grid. Therefore, if $\mathbf{r}_f$ represents the position of a grid point with respect to the fixed, inertial system, and if $\mathbf{r}'''$ represents the position of such a point in the grid-fixed system, an expression is required which gives $\mathbf{r}_f$ in terms of $\mathbf{r}'''$ and time. Then the time derivative of $\mathbf{r}_f$ will give the grid velocity. It should be noted that this exercise is the opposite of that which is commonly performed in a kinematics problem, for example, where velocities and accelerations are generally written with respect to a body-fixed system.

On an actual helicopter rotor, the flapping motion arises as a consequence of unequal lift forces at various azimuthal angles due to both unsymmetrical inflow and cyclic control inputs. To determine the amount of flapping and the aerodynamic forces at any azimuth, solution of a system coupling the blade dynamics with the aerodynamics is required. Such a procedure is far too time consuming for the current task, and, for this reason, a flapping motion considered

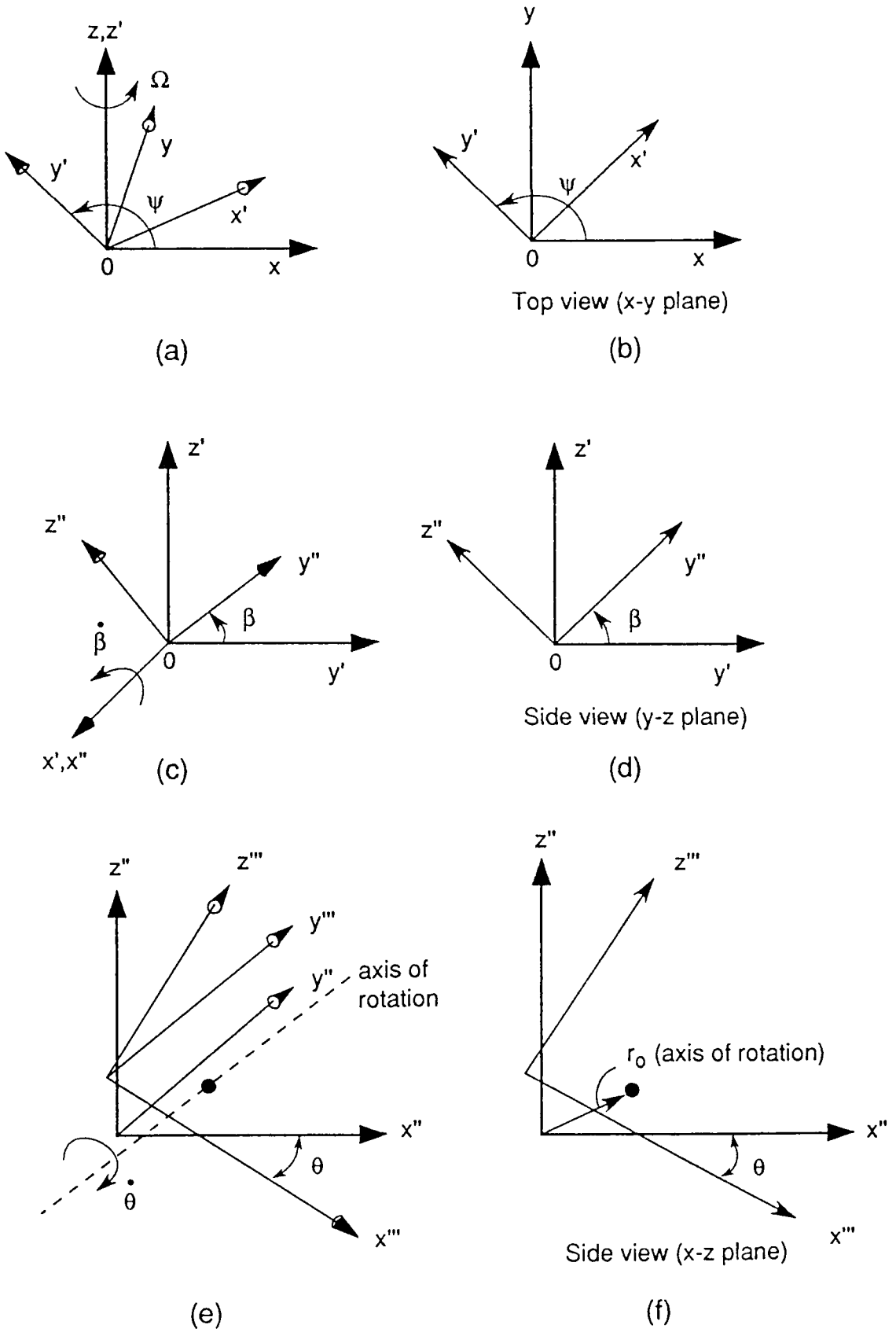

Figure 10: Definition of Coordinates for Feathering/Flapping Derivation

reasonable for the conditions under study is prescribed. In general, flapping and feathering are described in terms of Fourier series in ψ, the azimuth angle, as

$$\theta = \theta_0 + A_1 \cos\psi + B_1 \sin\psi + A_2 \cos 2\psi + B_2 \sin 2\psi + \ldots, \tag{5}$$

$$\beta = \beta_0 + a_1 \cos\psi + b_1 \sin\psi + a_2 \cos 2\psi + b_2 \sin 2\psi + \ldots, \tag{6}$$

where θ represents the pitching angle (feathering) and β the flapping angle. The current work restricts θ and β to their first harmonics, though the derivation of the grid velocities itself is general enough to include any specification of the pitching and flapping motion.

Consider the (x''', y''', z''') coordinates, shown in figure 10e, to be fixed to the grid (in this case, to the blade, also) such that y''' extends along the spanwise, or radial, direction and x''' runs in the chordwise direction, positive toward the trailing edge. The blade, and grid, pitch about an axis parallel to the y'''-axis, designated by the position vector, $\mathbf{r}_0$. Note that the vector, $\mathbf{r}_0$, is then the same in the (x''', y''', z''') system and the (x'', y'', z'') system, whose y-coordinate coincides with y''', but which does not pitch with the blade. Therefore, the triple-primed coordinates pitch about the axis, $\mathbf{r}_0$, with respect to the double-primed coordinates, with pitching rate $\dot{\theta}$. The relationship between a point, $\mathbf{r}''$, and a point given by $\mathbf{r}'''$ is then

$$\mathbf{r}'' = \mathbf{r}_0 + [H(\theta)]\,(\mathbf{r}''' - \mathbf{r}_0), \tag{7}$$

where $H(\theta)$ is a rotation matrix between the two systems. Now, the (x'', y'', z'') coordinates flap with respect to a system designated by (x', y', z'), whose x-axis coincides with x'', as shown in figure 10c. The relationship between $\mathbf{r}'$ and $\mathbf{r}''$ is then

$$\mathbf{r}' = [B(\beta)]\,\mathbf{r}'' \tag{8}$$

where $B(\beta)$ represents the flapping rotation matrix. In a similar manner,

$$\mathbf{r} = [S(\psi)]\,\mathbf{r}', \tag{9}$$

where, again, $S(\psi)$ transforms from a rotating (and translating) system to one which is just translating. (See figure 10a.) Note that the (x, y, z) system is translating with respect to

fixed space at a constant velocity, V which may approach at an angle, α, so that the velocity of the (x, y, z) coordinates with respect to the fixed ones will be $\mathbf{V} = -V\cos\alpha\hat{x} + V\sin\alpha\hat{y}$. In general, then

$$\mathbf{r}_f = \mathbf{r} + \mathbf{V}t. \tag{10}$$

The f subscripts refer to the space-fixed coordinates. To determine the grid velocities, note that

$$\dot{\mathbf{r}}_f = \dot{\mathbf{r}} + \mathbf{V}. \tag{11}$$

Now,

$$\mathbf{r} = [S(\psi)][B(\beta)]\{\mathbf{r}_0 + H(\theta)(\mathbf{r}''' - \mathbf{r}_0)\}, \tag{12}$$

so that,

$$\dot{\mathbf{r}} = [\dot{S}B]\mathbf{r}_0 + [S\dot{B}H](\mathbf{r}''' - \mathbf{r}_0). \tag{13}$$

The rotation matrices are all functions of time according to the prescribed feathering, flapping, and rotation motions which, up to this point in the derivation, can be considered perfectly general. The code utilized here considers only motion given by the first harmonics of equations 5 and 6, and rotation given by $\psi = \Omega t$.

The code which performs the flow calculations requires only the current grid positions, $\mathbf{r}$ or $\mathbf{r}_f$, and not those in the grid-fixed frame. To reduce the storage requirement---that is, so as to not have to store $\mathbf{r}'''$—the code solves eq. 12 for $\mathbf{r}'''$ in terms of $\mathbf{r}$ at each time step and then substitutes into eq. 13 to get the grid velocities in terms of $\mathbf{r}$ and $\mathbf{r}_0$ only.